SYNTHETIC BIOLOGY

Complex signal processing in synthetic gene circuits using cooperative regulatory assemblies

Caleb J. Bashor[1]*, Nikit Patel[2]*, Sandeep Choubey[3], Ali Beyzavi[4], Jané Kondev[3], James J. Collins[5,6,7], Ahmad S. Khalil[2,7]†

Eukaryotic genes are regulated by multivalent transcription factor complexes. Through cooperative self-assembly, these complexes perform nonlinear regulatory operations involved in cellular decision-making and signal processing. In this study, we apply this design principle to synthetic networks, testing whether engineered cooperative assemblies can program nonlinear gene circuit behavior in yeast. Using a model-guided approach, we show that specifying the strength and number of assembly subunits enables predictive tuning between linear and nonlinear regulatory responses for single- and multi-input circuits. We demonstrate that assemblies can be adjusted to control circuit dynamics. We harness this capability to engineer circuits that perform dynamic filtering, enabling frequency-dependent decoding in cell populations. Programmable cooperative assembly provides a versatile way to tune the nonlinearity of network connections, markedly expanding the engineerable behaviors available to synthetic circuits.

Cooperativity is a widespread biological phenomenon by which coordinated behavior within a molecular system emerges from energetic coupling between its components (*1*, *2*). In eukaryotic gene networks, cooperative assembly occurs when core initiation machinery is recruited to basal promoter regions through multivalent, mutually reinforcing interactions between transcription factors (TFs) and associated cofactors (*3*) (Fig. 1A). The resulting nucleoprotein complexes play a critical signal-processing and decision-making role (*4*–*11*); they convert analog TF inputs into switch-like transcriptional outputs (*12*, *13*) or incorporate multiple TFs to carry out decision functions by activating transcription only in the presence of TF combinations (*4*, *14*).

To date, most synthetic gene circuits have been constructed by using TFs that bind to promoters in a one-to-one fashion (*15*–*17*), constraining the ability to tune circuit cooperativity and potentially imposing limits on engineerable behavior (*18*) (Fig. 1A, top). We asked whether circuits with expanded signal-processing function can be implemented by using engineered multivalent assembly (Fig. 1A, bottom). We established theoretical and design frameworks for programming cooperative TF assembly on the basis of the configuration and strength of intracomplex interactions and constructed synthetic gene circuits composed of interconnected regulatory assemblies.

In our scheme for engineering cooperative TF assemblies (Fig. 1B), transcription is activated when synthetic zinc finger (ZF) proteins fused to transcriptional activator domains (synTFs) bind tandem DNA binding motifs (DBMs) located upstream of a core promoter (*19*, *20*). Assembly is mediated by a "clamp" protein: multiple covalently linked PDZ domains that bind peptide ligands located on the C termini of adjacent DBM-bound synTFs. Complex free energy can be adjusted by varying either the number of clamp-synTF-DBM repeats (n_c) or the affinities of synTF-DBM and PDZ-ligand interactions (K_t and K_p, respectively), which is enabled by affinity variants for both domains (15 ZF-DNA and 13 PDZ-ligand interactions) (figs. S2 and S3).

To directly test whether the synTF-clamp-DBM module can support cooperative assembly,

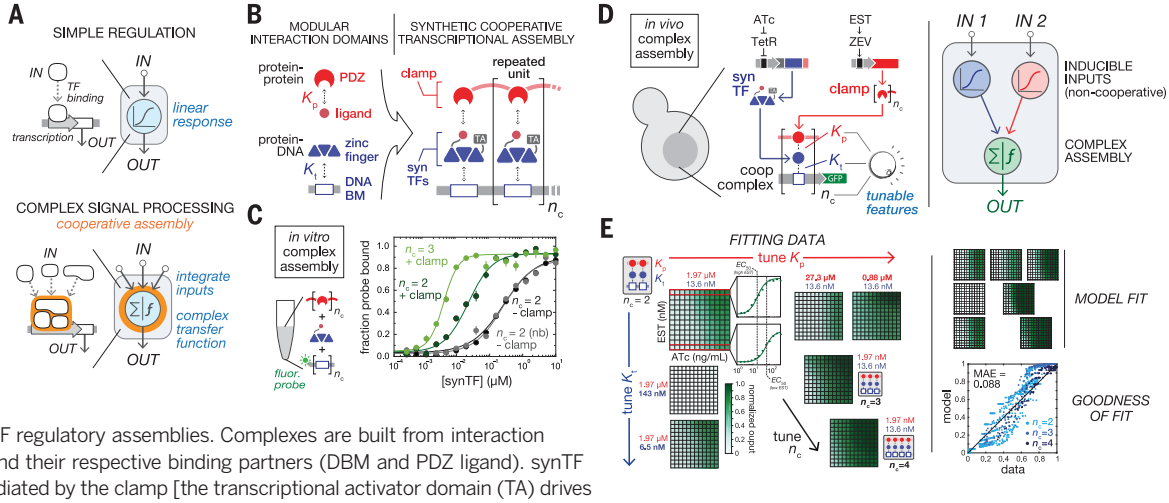

Fig. 1. Design scheme for assembly-mediated regulatory control of synthetic gene circuits. (**A**) Nodes in cellular networks use one-to-one regulatory interactions to execute simple computational tasks (top); cooperative interactions within multivalent assemblies enable complex, nonlinear signal processing (bottom). (**B**) Design of synthetic TF regulatory assemblies. Complexes are built from interaction domains (ZF and PDZ) and their respective binding partners (DBM and PDZ ligand). synTF complex formation is mediated by the clamp [the transcriptional activator domain (TA) drives coding sequence transcription]. Interaction affinities (K_t and K_p) and the number of repeated complex units (n_c) determine the thermodynamics of assembly. (**C**) In vitro assembly of purified cooperative complex components. Fluorescence anisotropy for a synTF titration against a DBM oligonucleotide probe (fluorescein isothiocyanate labeled) was measured in the presence or absence of clamp (5 μM) and converted into the fraction of probe bound (see supplementary materials and methods). Fluor., fluorescent; nb, synTFs with binding-deficient PDZ ligand mutants; n_c, number of PDZ domains per clamp and DBM probe. Points represent mean values for three measurements ± SE. (**D**) Testing in vivo complex assembly in yeast by using a synthetic gene circuit (GFP output). All genes are chromosomally integrated (left) (see table S3). The small molecule–inducible expression systems ncTET and ncZEV control intracellular expression levels (see fig. S4) of the synTF (induced by ATc, 2 to 500 ng/ml) and clamp (induced by EST, 0.05 to 12.5 nM), respectively. Adjusting the molecular features of assembly (K_t, K_p, and n_c) tunes overall circuit transfer function (right). coop, cooperative; TetR, Tn*10* tetracycline repressor; ZEV, zinc finger–estrogen receptor–VP16 activator; Σ, input integration; *f*, transfer function. (**E**) Parameterization of the thermodynamic complex assembly model. Dose-response data for circuit configurations with various K_t, K_p, and n_c values were fit to a thermodynamic model (figs. S7 and S8 and supplementary materials and methods); a regression plot showing the residual from fit is shown at the right. MAE, mean absolute error.

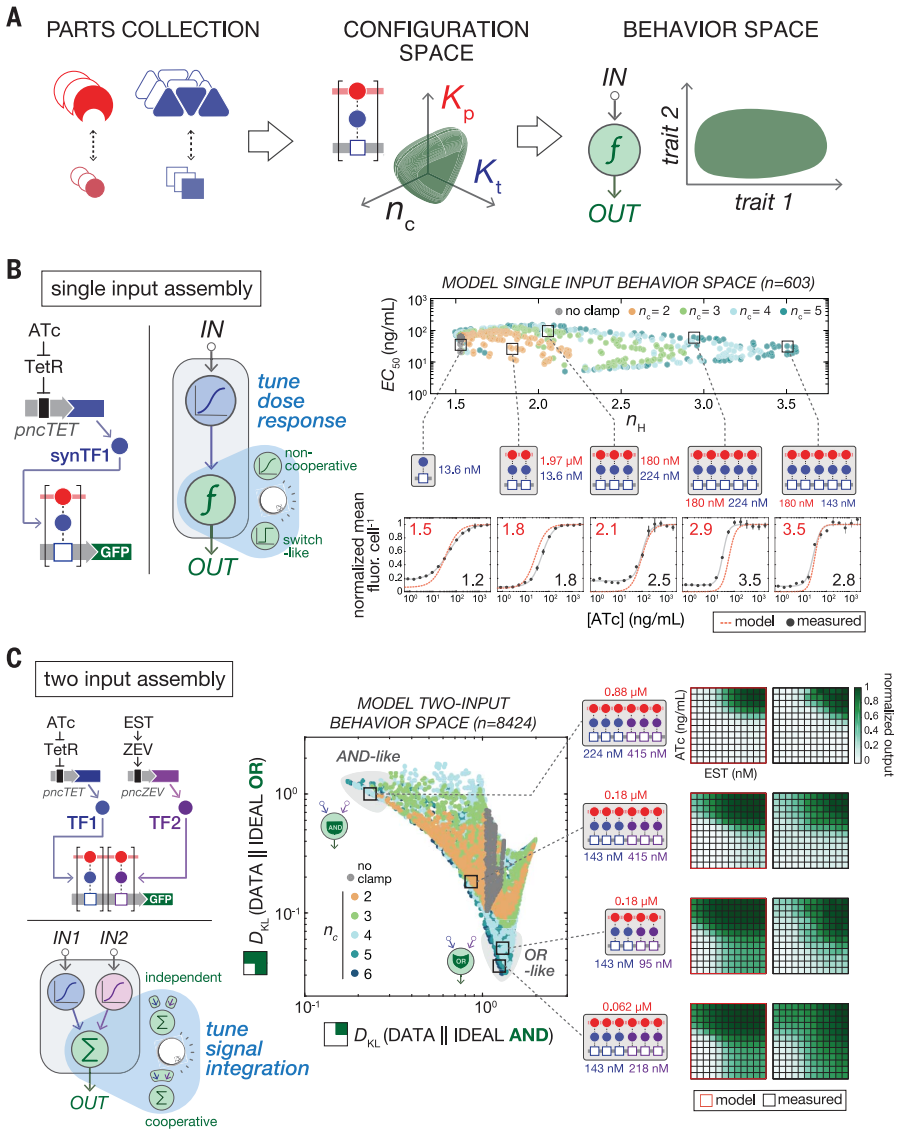

Fig. 2. Constructing gene circuits by using cooperative TF assemblies enables expanded steady-state signal-processing behavior. (**A**) Computational model–driven approach for exploring engineerable circuit behavior. Our parts collection (left) defines available configuration space (middle). K_p, PDZ-ligand variants; K_t, synTF-DBM variants; n_c, clamp-synTF-DBM units. Our model (figs. S7 to S9) computes input-output functions for this space, mapping the potential circuit behavior range (behavior space) (right). *f*, transfer function. (**B**) Programmed complex assembly enables tuning of a single-input circuit dose response. For a single-input (two-node) circuit, the synTF is induced by ATc addition (input node) and assembles with constitutively expressed clamp to regulate GFP transcription (reporter node) (left). In model-computed circuit behavior space (right), colors indicate different complex sizes (n_c). Five circuits with different assemblies [with parameters K_t affinity (blue), K_p affinity (red), and n_c] were constructed and tested by inducing with ATc and measuring GFP by flow cytometry after 16 hours (below). Points represent mean values for three experiments ± SE. pncTET, ncTET-regulated promoter; fluor., flourescence. (**C**) Programmed complex assembly enables tuning of two-input dose response between linear and nonlinear computations. In a two-input circuit, synTF1 (TF1) and synTF2 (TF2) are induced by ATc and EST, respectively (input nodes), assembling with constitutively expressed clamp to regulate a downstream reporter node (left). The behavior space for the full set of available circuit configurations (center) is plotted as K-L divergence (D_{KL}): "similarity" between model-computed output surfaces and archetypal Boolean AND and OR surfaces (see fig. S13). Gray areas in the plot indicate regions of AND- and OR-like behavior. Selected circuits, with corresponding reporter complex parameters [K_t affinity (blue), K_p affinity (red), and n_c], were constructed, and their 2D output surfaces were experimentally measured (right) by inducing with ATc and EST and measuring GFP by flow cytometry after 16 hours (see supplementary materials and methods). pncZEV, ncZEV-regulated promoter.

we conducted in vitro fluorescence anisotropy binding experiments on purified complex components (figs. S2 and S3 and supplementary materials and methods). synTF binding to an n_c = 2 probe showed a noncooperative dose-response profile, whereas the presence of a two-PDZ clamp lowered the synTF binding threshold and steepened the dose response, an effect not observed for a nonbinding synTF or for an n_c = 1 probe (Fig. 1C). Complex formation with an n_c = 3 probe (and a three-PDZ clamp) demonstrated a still sharper, lower-threshold response. Thus, synTF binding cooperativity is enhanced by the clamp and scales in magnitude with the complex size.

We next demonstrated in vivo complex assembly in yeast cells by constructing a transcriptional circuit in which an n_c = 2 synTF assembly drives a green fluorescent protein (GFP) reporter, with synTF and clamp levels controlled via noncooperative, small molecule–inducible expression systems (Fig. 1D and fig. S4): ncTET (for synTF expression) (*21*), induced with anhydrotetracycline (ATc), and ncZEV (for clamp expression) (*22*), induced with estradiol (EST). A dose-response surface was obtained by titrating ATc against EST and recording GFP fluorescence output by flow cytometry (Fig. 1E, upper left). Consistent with clamp-enhanced synTF binding, the ATc dose-response threshold was reduced in the presence of increasing EST (Fig. 1E).

To quantitatively describe complex formation, we formulated a simple statistical thermodynamic model (*14*, *23*, *24*) relating intracellular synTF and clamp expression to promoter occupancy and resulting GFP output (figs. S7 to S10; see supplementary text for the full model description). The model was fit to experimental two-input dose-response data for seven complex configurations, where K_t, K_p, and n_c were experimentally adjusted (Fig. 1E). Parameter fitting was constrained by in vitro–measured PDZ and ZF interaction affinities (figs. S2 and S3) and inducible-component expression data (fig. S4). The fitted model can be used to guide circuit engineering, enumerating potential circuit behaviors (behavior space) on the basis of input-output functions calculated for available

[1]Department of Bioengineering, Rice University, Houston, TX 77030, USA. [2]Department of Biomedical Engineering and Biological Design Center, Boston University, Boston, MA 02215, USA. [3]Department of Physics, Brandeis University, Waltham, MA 02453, USA. [4]Department of Mechanical Engineering, Boston University, Boston, MA 02215, USA. [5]Institute for Medical Engineering and Science, Department of Biological Engineering, and Synthetic Biology Center, Massachusetts Institute of Technology, Cambridge, MA 02139, USA. [6]Broad Institute of MIT and Harvard, Cambridge, MA 02142, USA. [7]Wyss Institute for Biologically Inspired Engineering, Harvard University, Boston, MA 02115, USA.
*These authors contributed equally to this work.
†Corresponding author. Email: khalil@bu.edu

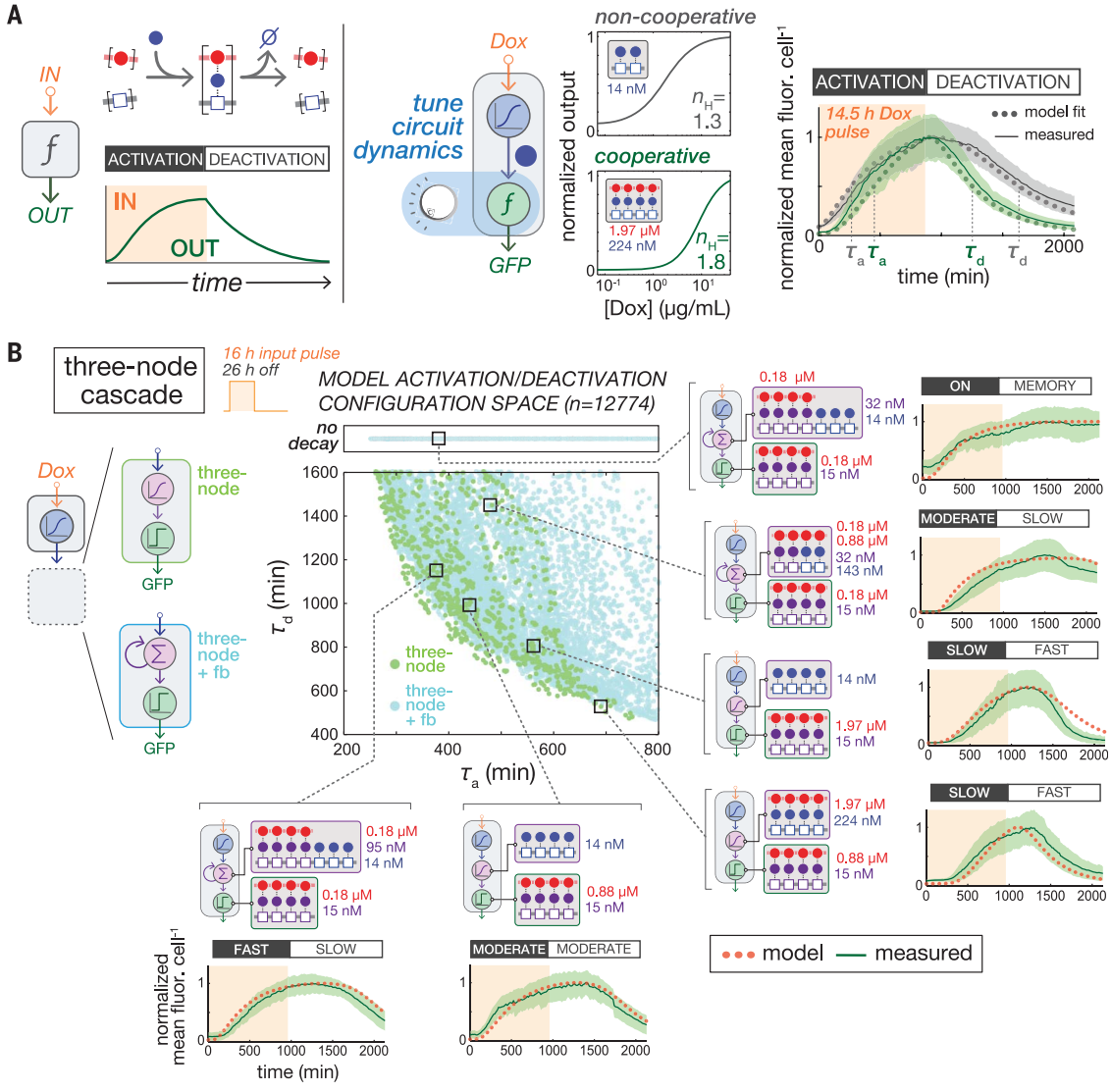

Fig. 3. Controlling gene circuit dynamics by using programmed complex assembly. (**A**) Tuning assembly cooperativity to control phases of circuit activation. synTF complex formation (left) determines circuit activation and deactivation kinetics (green) in response to transient inducer input (orange). Model-generated dose-response profiles for two-node cascades regulated by noncooperative two-TF (gray) or cooperative four-TF (green) assemblies are shown. Data from time course experiments using time-lapse microscopy in a microfluidic device [lines = mean fluorescence intensity (fluor.) per cell; shaded boundaries = ±1 SD of the population mean; τ_a, activation half-time; τ_d, deactivation half-time] were compared with model-fitted behavior (dots) (see supplementary materials and methods). *f*, transfer function. (**B**) Cooperative assemblies enable the activation and decay phases to be broadly and independently tuned for a three-node cascade motif. The model-predicted dynamic behavior space compares τ_a and τ_d for three-node motifs with (light blue) and without (light green) feedback (fb) ("no decay" indicates configurations that did not return to basal activity upon input removal). Highlighted circuits were tested by time-lapse microscopy with microfluidics (16 hours of Dox induction, light orange; lines = mean fluorescence intensity per cell normalized to maximum output; shaded boundaries = ±1 SD) and compared with model simulations (dots). See movies S1 and S2 for time-lapse videos.

configurations of parts (configuration space) (Fig. 2A and figs. S2 to S4).

We examined dose-response behavior for a single-input (two-node) circuit motif consisting of an inducible upstream input node (driving synTF production) and a downstream reporter node where the synTF assembles with a constitutively expressed clamp (Fig. 2B). We asked whether features of the circuit dose response—the half-maximal dose response (EC_{50}) and Hill coefficient (n_H)—could be systematically tuned by adjusting complex K_t, K_p, and n_c (Fig. 2B and fig. S11). Dose responses for all part-allotted configurations (603) were computed, and EC_{50} and n_H values were plotted as a two-dimensional (2D) behavior space (Fig. 2B and fig. S12). Low-valency configurations conferred linear (lower-n_H) dose responses, whereas those with higher n_c values were broadly distributed, including configurations exhibiting the most switchlike (n_H > 3.0) behavior (fig. S12). Circuit configurations with different predicted n_H values were tested experimentally (fig. S12) and showed good correspondence with the model (Fig. 2B and fig. S12C).

We next assessed the relationship between assembly and Boolean computation for complexes integrating multiple synTF inputs (TF1 and TF2, respectively controlled by ncTET and ncZEV) (Fig. 2C). We calculated dose-response surfaces for two-input circuits containing complexes ranging from n_c = 2 to 6 for all possible combinations of TF1 and TF2 occupancy and

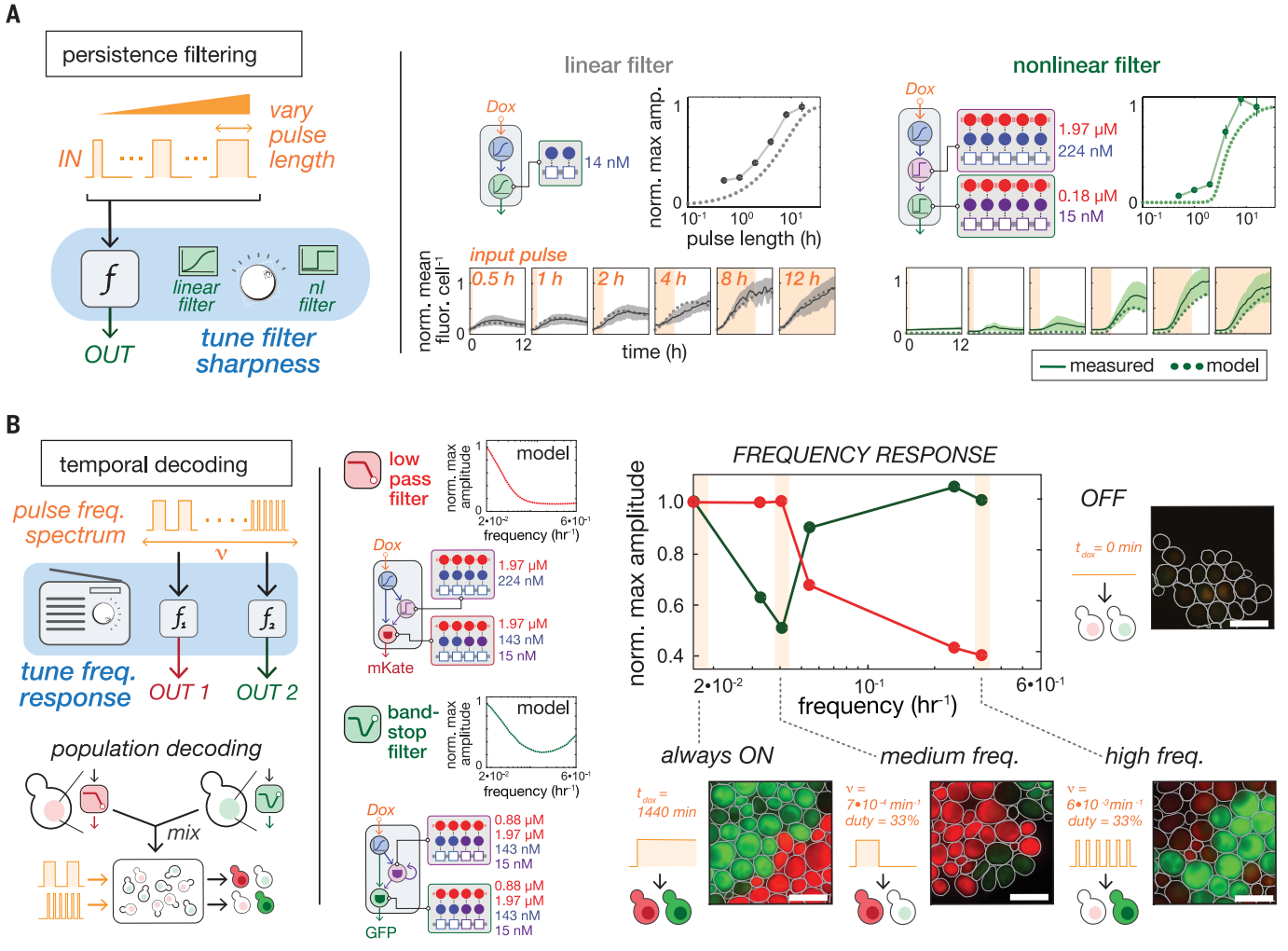

Fig. 4. Circuits engineered with cooperative assemblies perform temporal signal-processing behavior. (**A**) Persistence filtering in cooperative assembly circuits. Computationally identified two- and three-node motifs reveal persistence filtering behavior: activation in response to an input of a sufficient duration (left) (fig. S21). Circuits predicted to show linear (shallow) (gray) and nonlinear (sharp) (green) filtering were tested in microfluidic time course experiments [lines = mean fluorescence intensity (fluor.) per cell; shaded region = ±1 SD of the cell population] by inducing with increasing Dox pulse lengths (light orange). Temporal dose-response curves (line = measured data; dots = model) were generated from normalized (norm.) time course output maxima (see supplementary materials and methods). *f*, transfer function; nl, nonlinear; max amp., maximum amplitude. (**B**) Population-level temporal decoding of frequency (freq.) input. Computationally identified (fig. S22) two- and three-node network motifs (left) were tested for frequency filtering behavior in microfluidic experiments. Mixed populations of yeast harboring LPF and BSF feed-forward circuits (driving mKate and GFP, respectively) were tested for their ability to decode a frequency-modulated square wave of Dox pulses (fig. S23). Model-predicted frequency responses are shown next to each circuit. The experimentally measured frequency response is shown to the right. The maximum reporter output for each input frequency was normalized to the maximum output for constitutive Dox (fig. S22). Representative mixed-population fluorescence images are shown for frequencies highlighted in orange: constitutive Dox (always on), medium-frequency treatment (~10^{-5} Hz; 33%), and high frequency (~10^{-4} Hz; 33%). Cells without Dox treatment (off) are shown to the right. In images, cells harboring LPF and BSF circuits are false-colored red and green, respectively; cell boundaries were determined by segmentation software (see supplementary materials and methods). t_{dox}, Dox pulse duration; ν, frequency. Scale bars, 10 μM.

interaction affinity (8424 in total) (fig. S13A). We used Kullback-Leibler (K-L) divergence to compare idealized digital AND- and OR-like logic functions with simulated circuit behaviors (fig. S13, B and C). Plotting K-L divergences as a scatter revealed that regions of behavior space containing the most nonlinear, Boolean-like circuits generally contained higher-order (n_c > 3) assemblies (Fig. 2C and fig. S14). Circuits representing different regions of configuration space were constructed and tested, with most performing in model-predicted fashion (fig. S15), including those from AND- and OR-like regions (Fig. 2C).

Because the timing of complex assembly is dependent on the rate of synTF accumulation, we hypothesized that assembly configuration could be adjusted to control circuit dynamics (Fig. 3A). Using time-lapse fluorescence microscopy analysis of microfluidic device–cultured yeast (supplementary materials and methods), we measured circuit GFP expression in response to transient doxycycline (Dox) inducer pulses (fig. S16). We extended our model to account for temporal circuit behavior by fitting the model to time course experiments (fig. S17, A and B, and supplementary text). We highlight two fitted circuits: an n_c = 2 complex that exhibits a noncooperative steady-state dose response, and one with a more cooperative n_c = 4 complex (Fig. 3A). The latter exhibits a delayed activation onset and rapid decay upon Dox removal, demonstrating that the timing of circuit activation and deactivation

phases can be tuned by adjusting complex cooperativity.

We analyzed circuit dynamics behavior space for three-node cascades in which two distinct synTF assemblies connected in series (Fig. 3B), examining the basis of apparent half-time for circuit activation (τ_a) and decay (τ_d). We considered circuits with two middle node configurations: one with an assembly containing a single synTF and the other where the promoter was also under positive autoregulation by its own output synTF. Plotting of simulated dynamics for part-permitted three-node behavior space (12,774 configurations) revealed a broad distribution of temporal behaviors (Fig. 3B and fig. S18), with circuits composed of cooperative, higher-n_c assemblies demonstrating the broadest τ_a and τ_d tuning (fig. S19). Only positive-feedback configurations could access both slow activation–slow decay behavior and stable memory (no decay), suggesting circuit sensitivity to TF integration at the middle node of the cascade (Fig. 3B). We selected circuit configurations located throughout the behavior space to test experimentally; performance of these circuits confirmed the model's ability to describe the range of temporal behaviors that can be achieved (Fig. 3B, fig. S20, and movies S1 and S2).

Cellular networks are capable of responding to information encoded in the dynamics of an input signal (*25*, *26*), responding to inputs of a specific duration (*27*), or decoding features of an input time series (e.g., frequency) (*28*). To demonstrate that cooperative assemblies could facilitate the engineering of dynamic filtering behavior, we computationally identified two- and three-node motifs (fig. S21A) capable of persistence filtering—activation only in the presence of a sufficiently long duration input (Fig. 4A). Filtering behavior with a steep duration-dependent threshold was exhibited by three-node cascades with cooperative, high-n_c complexes (fig. S21B). Results of Dox pulse titration experiments were consistent with these predictions: A two-node circuit with a low-valency assembly demonstrated linear filtering, whereas a three-node circuit with highly cooperative assemblies showed sharp filtering (Fig. 4A).

As a final demonstration, we engineered sets of circuits capable of differentially responding to distinct input frequencies (Fig. 4B). We computationally identified a pair of circuits, both coherent feed-forward loops, activated by distinct square-wave frequencies (fig. S22). These included low-pass filters (LPFs), which respond only to low-frequency input, and band-stop filters (BSFs), which filter medium frequency while activating at high frequency (both with a 33% duty cycle). For both circuits, cooperative, high-n_c assemblies were critical for sharp filtering (fig. S22C). To test filtering function, we created two strains: a BSF circuit driving a GFP reporter and an LPF with an mKate reporter. As predicted, at different input frequencies, strains differentially activated within a mixed population (BSF at ~10^{-4} Hz; LPF at ~10^{-5} Hz) (Fig. 4B and fig. S23).

Our work demonstrates that cooperative assembly is a powerful, highly flexible design strategy for engineering nonlinear circuit behavior and offers clues as to why TF assemblies evolved as a dominant mode of transcriptional regulatory control (*29*, *30*). Adjusting promoter assemblies may have provided networks with a simple way to interpolate between diverse regions of functional space (*31*, *32*). Use of engineering approaches that incorporate cooperative assembly could facilitate the creation of signal-processing circuitry (*33*), enabling precision control in applications where nonlinear temporal and spatial signal processing are critical, such as circuit-directed cell differentiation or the dynamic regulation of homeostasis in engineered tissues.

REFERENCES AND NOTES

1. A. V. Hill, *J. Physiol.* **40**, iv–vii (1910).
2. A. Whitty, *Nat. Chem. Biol.* **4**, 435–439 (2008).
3. M. Ptashne, *Nature* **335**, 683–689 (1988).
4. Y. E. Antebi *et al*., *Cell* **170**, 1184–1196.e24 (2017).
5. U. S. Bhalla, R. Iyengar, *Science* **283**, 381–387 (1999).
6. J. E. Ferrell Jr., S. H. Ha, *Trends Biochem. Sci.* **39**, 612–618 (2014).
7. M. Levine, *Curr. Biol.* **20**, R754–R763 (2010).
8. F. Spitz, E. E. Furlong, *Nat. Rev. Genet.* **13**, 613–626 (2012).
9. K. Struhl, *Neuron* **7**, 177–181 (1991).
10. J. R. Williamson, *Nat. Chem. Biol.* **4**, 458–465 (2008).
11. Q. Zhang, S. Bhattacharya, M. E. Andersen, *Open Biol.* **3**, 130031 (2013).
12. M. Carey, *Cell* **92**, 5–8 (1998).
13. R. A. Veitia, *Biol. Rev. Cambridge Philos. Soc.* **78**, 149–170 (2003).
14. N. E. Buchler, U. Gerland, T. Hwa, *Proc. Natl. Acad. Sci. U.S.A.* **100**, 5136–5141 (2003).
15. C. J. Bashor, A. A. Horwitz, S. G. Peisajovich, W. A. Lim, *Annu. Rev. Biophys.* **39**, 515–537 (2010).
16. J. A. Brophy, C. A. Voigt, *Nat. Methods* **11**, 508–520 (2014).
17. P. E. Purnick, R. Weiss, *Nat. Rev. Mol. Cell Biol.* **10**, 410–422 (2009).
18. N. E. Buchler, F. R. Cross, *Mol. Syst. Biol.* **5**, 272 (2009).
19. A. J. Keung, C. J. Bashor, S. Kiriakov, J. J. Collins, A. S. Khalil, *Cell* **158**, 110–120 (2014).
20. A. S. Khalil *et al*., *Cell* **150**, 647–658 (2012).
21. D. Nevozhay, R. M. Adams, K. F. Murphy, K. Josic, G. Balázsi, *Proc. Natl. Acad. Sci. U.S.A.* **106**, 5123–5128 (2009).
22. R. S. McIsaac *et al*., *Nucleic Acids Res.* **41**, e57 (2013).
23. H. G. Garcia, J. Kondev, N. Orme, J. A. Theriot, R. Phillips, *Methods Enzymol.* **492**, 27–59 (2011).
24. J. Gertz, E. D. Siggia, B. A. Cohen, *Nature* **457**, 215–218 (2009).
25. J. H. Levine, Y. Lin, M. B. Elowitz, *Science* **342**, 1193–1200 (2013).
26. J. E. Purvis, G. Lahav, *Cell* **152**, 945–956 (2013).
27. S. Mangan, U. Alon, *Proc. Natl. Acad. Sci. U.S.A.* **100**, 11980–11985 (2003).
28. A. Mitchell, P. Wei, W. A. Lim, *Science* **350**, 1379–1383 (2015).
29. D. Hnisz, K. Shrinivas, R. A. Young, A. K. Chakraborty, P. A. Sharp, *Cell* **169**, 13–23 (2017).
30. J. Zhu, Y. Shang, M. Zhang, *Nat. Rev. Neurosci.* **17**, 209–223 (2016).
31. C. R. Baker, L. N. Booth, T. R. Sorrells, A. D. Johnson, *Cell* **151**, 80–95 (2012).
32. B. B. Tuch, H. Li, A. D. Johnson, *Science* **319**, 1797–1799 (2008).
33. N. Novershtern *et al*., *Cell* **144**, 296–309 (2011).

ACKNOWLEDGMENTS

We thank J. K. Joung and members of the Collins and Khalil laboratories for helpful discussions. **Funding:** This work was supported by NSF Expeditions in Computing grant CCF-1522074 (A.S.K.) and DARPA grant W911NF-11-2-0056 (J.J.C. and A.S.K.). A.S.K. also acknowledges funding from the NIH director's New Innovator award (1DP2AI131083-01), an NSF CAREER award (MCB-1350949), and a DARPA Young Faculty award (D16AP00142). **Author contributions:** C.J.B., N.P., and A.S.K. conceived the study. C.J.B. and N.P. prepared materials and performed all experiments. N.P. and S.C. performed theoretical modeling. A.B. designed and fabricated microfluidic devices, and N.P. performed microfluidic experiments. J.K., J.J.C., and A.S.K. oversaw the study. C.J.B., N.P., and A.S.K. wrote the manuscript. **Competing interests:** C.J.B., N.P., J.J.C., and A.S.K. are inventors on U.S. provisional patent application 62/691,187, filed 28 June 2018 by Boston University. **Data and materials availability:** All DNA constructs and cell strains are available from A.S.K. The datasets generated and analyzed and the computer code used during the current study are available upon request from the corresponding author.

SUPPLEMENTARY MATERIALS

science.sciencemag.org/content/364/6440/593/suppl/DC1
Materials and Methods
Supplementary Text
Figs. S1 to S24
Tables S1 to S4
References (*34*–*54*)
Movies S1 and S2

18 July 2018; accepted 3 April 2019
Published online 18 April 2019
10.1126/science.aau8287

Complex signal processing in synthetic gene circuits using cooperative regulatory assemblies

Caleb J. Bashor, Nikit Patel, Sandeep Choubey, Ali Beyzavi, Jané Kondev, James J. Collins and Ahmad S. Khalil

Science **364** (6440), 593-597.
DOI: 10.1126/science.aau8287originally published online April 18, 2019

Cooperativity in synthetic gene circuits

Synthetic biologists would like to be able to make gene regulatory circuits that mimic key properties of eukaryotic gene regulation. Taking a cue from multimeric transcription factor complexes, Bashor *et al.* developed synthetic transcriptional circuits that produce nonlinear behavior from cooperativity (see the Perspective by Ng and El-Samad). Their system uses clamp proteins with multiple protein-interaction domains. Circuit behavior can be tuned by altering the number or affinities of the interactions according to a mathematical model. The authors created synthetic circuits with desired functions common in biology, for example, switch-like behavior or Boolean decision functions.

Science, this issue p. 593; see also p. 531